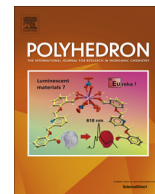




Contents lists available at ScienceDirect

Polyhedron

journal homepage: www.elsevier.com/locate/poly

“Scorpionate-like” complexes that are held together by hydrogen bonds: Crystallographic and spectroscopic studies of (3-NH(*t*-butyl)-5-methyl-pyrazole)_nMX₂ (M = Zn, Ni, Co, Mn; *n* = 3, 4; X = Cl, Br)

Lee Serpas^a, Robert R. Baum^c, Alyssa McGhee^c, Ismael Nieto^a, Katherine L. Jernigan^e, Matthias Zeller^b, Gregory M. Ferrence^d, David L. Tierney^c, Elizabeth T. Papish^{a,e,*}

^a Drexel University, Dept. of Chemistry, 3141 Chestnut St., Philadelphia, PA 19104, United States

^b Youngstown State University, Dept. of Chemistry, One University Plaza, Youngstown, OH 44555, United States

^c Miami University, Dept. of Chemistry and Biochemistry, 701 East High Street, Oxford, OH 45056, United States

^d Illinois State University, Dept. of Chemistry, CB 4160, Normal, IL 61790, United States

^e The University of Alabama, Dept. of Chemistry, 250 Hackberry Lane, Tuscaloosa, AL 35401, United States

ARTICLE INFO

Article history:

Received 4 July 2015

Accepted 5 October 2015

Available online xxx

Keywords:

Hydrogen-bonds

Scorpionates

Transition metal complexes

Pyrazoles

Anion binding

ABSTRACT

The hydrogen bonding ligand, 3-NH(*t*-butyl)-5-methyl-pyrazole, forms “scorpionate-like” first row transition metal complexes that are held together by hydrogen bonds rather than covalent bonds. The formulae of these complexes are (LH)_nMX₂, where *n* = 3, 4; X = Cl, Br; and LH = 3-NH(*t*-butyl)-5-methyl-pyrazole. The amino-substituted pyrazole can hydrogen bond via both the amino group and the pyrazole NH to form intramolecular NH to halide hydrogen bonds. These complexes have been well characterized and show a 3:1 ratio of ligand to metal for zinc and cobalt (**1** and **2**), and a 4:1 ratio of ligand to metal for manganese and nickel (**3** and **4**). The hydrogen bonding interactions appear to be stronger for the 3:1 complexes. The crystallographic and spectroscopic studies (EPR and NMR) have shown that these hydrogen-bonding interactions are strong enough to perturb metal halogen bond distances and, with non-hydrogen bonding solvents, the hydrogen bonds appear to hold these complexes together in solution.

© 2015 Elsevier Ltd. All rights reserved.

1. Introduction

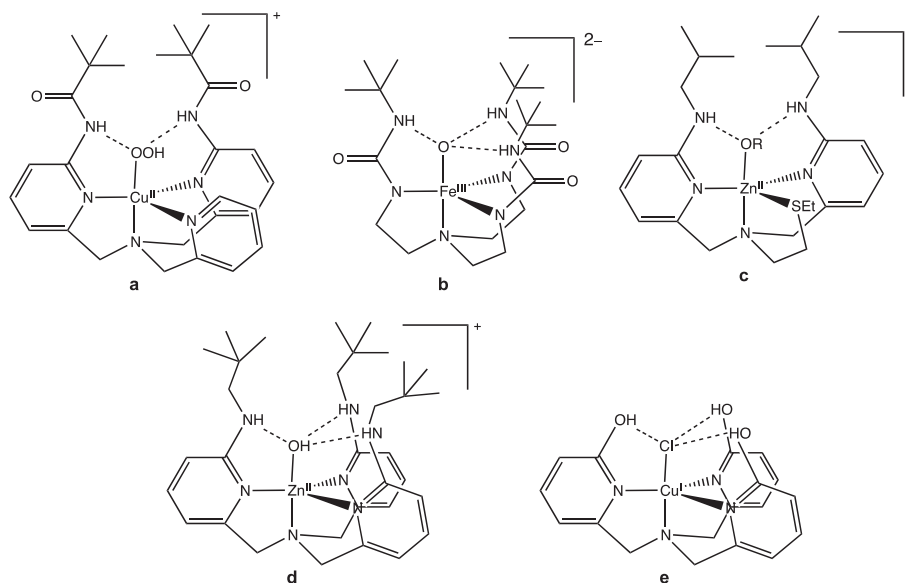
Hydrogen bonding motifs are found in many enzymes and are often responsible for determining biological function [1]. They also provide an important design principle for chemists wishing to mimic Nature’s selectivity and efficiency. For example, key differences in the presence or absence of hydrogen bond donors and acceptors determine why oxygen-bound peroxidase enzymes cleave the O–O bond but the globins bind and release oxygen, leaving the O–O bond intact [2,3]. Several different types of ligands have been designed to provide hydrogen bonds near the metal center [4,5]. Amide and urea groups have been used by Masuda [6] and Borovik [7], respectively, and these groups offer strong hydrogen bonds near the metal center on a tripodal scaffold (Scheme 1a and b). Berreau [8] and Mareque-Rivas [9] (Scheme 1c and d) have used amine hydrogen bonding groups to construct a similar

scaffold. These studies have shown that hydrogen bonds can tune the redox potentials of the bound metal [10,11], allow for the isolation of rare metal oxo complexes [12], and aid in the activation of water and CO₂ [13–15]. Recently, during the later stages of our study, a new ligand with a tripodal network of hydrogen bonds near the metal has been reported by Szymczak (Scheme 1e) [16]. However, all of the above species have supported trigonal-bipyramidal geometries at the metal center. We were intrigued with the possibility of a non-coordinating atom anchoring the hydrogen-bonding scaffold.

We have had a long-standing interest in creating scaffolds that place hydrogen bonds near and far from the metal center [17–24]. The work herein describes the synthesis of a novel tripodal, monoanionic ligand based upon amino substituted pyrazole rings (LH) that offers hydrogen bonds near the metal center. In the course of our synthetic efforts towards novel tripodal ligands, we discovered that 3-(NH-*t*-Butyl)-5-methyl-pyrazole (LH) can support metal complexes ((LH)_nMX₂) which contain a network of six to eight intramolecular hydrogen bonds. In particular, this study shows that hydrogen bonds alone can be used to bind anions,

* Corresponding author at: The University of Alabama, Dept. of Chemistry, 250 Hackberry Lane, Tuscaloosa, AL 35401, United States.

E-mail address: etpapish@ua.edu (E.T. Papish).



Scheme 1. Hydrogen bonding ligand scaffolds designed by Masuda (a), Borovik (b), Berreau (c), Mareque-Rivas (d), and Szymczak (e).

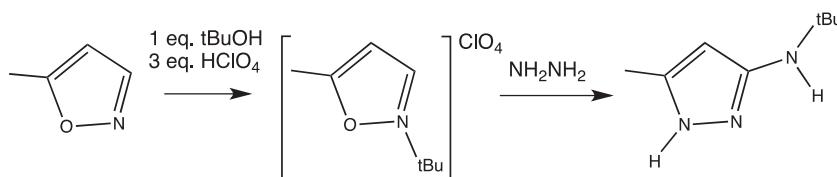
and metal to halide bonds are lengthened by hydrogen bonding interactions.

2. Results and discussion

2.1. Synthesis and ligand design

We used pyrazole-based ligands with amine groups at the three position for formation of a hydrogen bonding network. We were

encouraged by a report by Aullón et al. that demonstrated computationally that three-position amine groups (NH_2 in their case) were helpful for oxygen activation [25]. We chose instead to use $\text{NH}(\text{t-butyl})$ groups for steric protection of the metal center. We initially aimed to synthesize chelates, as described in the supporting information, but these initial efforts were unsuccessful. In the course of these studies we discovered that 3- $\text{NH}(\text{t-butyl})$ -5-methyl-pyrazole (LH) supports structures with intramolecular hydrogen bonds that are interesting in their own right.



Scheme 2. The synthesis of 3- $\text{NH}(\text{t-butyl})$ -5-methyl-pyrazole.

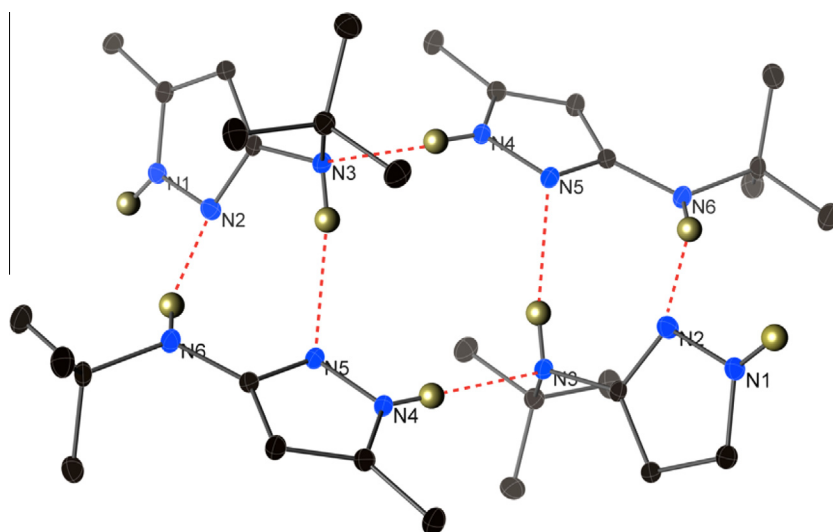
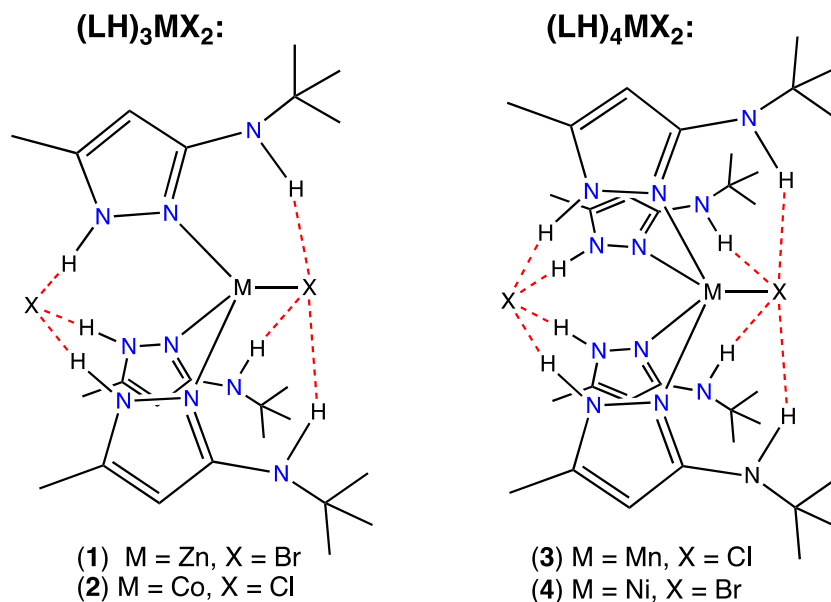


Fig. 1. Structural diagram for the tetramer of 3- (NH-t-Butyl) -5-methyl-pyrazole (LH). Ellipsoids are shown at 30% probability. Hydrogen bonds (red dashed lines) connect four pyrazole molecules (two asymmetric units). Non-hydrogen bonding hydrogen atoms are omitted for clarity. (Colour online.)



Scheme 3. The products formed from attempts to coordinate $\text{Ti}(\text{L}_3\text{BH})$ to a transition metal. Combining excess LH and MX_2 in solution also forms these products. Hydrogen bonds are shown in red. Note that for complex **4**, short contacts between NH and Br are present, but these are too long to be hydrogen bonds. (Colour online.)

We began by synthesizing the pyrazole ring (LH) as described in the literature (Scheme 2) [26]. Steps 1 and 2 were achieved in 95% and 96% yields, respectively. The product pyrazole was characterized by ^1H and ^{13}C -NMR, IR and MS, and all spectra matched the literature report. This pyrazole was crystallized from toluene, and the X-ray crystal structure is described below (see Section 2.2, Fig. 1).

The $(\text{LH})_n\text{MX}_2$ products (**1–4**) can be formed in high yields and remarkably, they resemble scorpionate complexes but they are held together only by hydrogen bonds and coordinate-covalent ligand to metal interactions (Scheme 3). These complexes can also

be regarded as self-assembled molecular structures. The $\text{M} = \text{Zn}^{\text{II}}$, Co^{II} complexes (**1**, **2**, respectively) show a *three to one* ratio of ligand to metal and are characterized by spectroscopic and analytical methods (with crystal structures obtained). The $\text{M} = \text{Mn}^{\text{II}}$, Ni^{II} complexes (**3**, **4**, respectively) show a *four to one* ratio of ligand to metal and all are characterized by spectroscopic, analytical, and crystallographic methods. The reasons for these coordination preferences appear to be related to the size of the ionic radii (Zn^{II} is the smallest ion and prefers a tetrahedral structure; conversely Mn^{II} is largest). Crystal field stabilization also reaches a maximum for Ni^{II} among first row divalent ions [27–31] and would favour a

Table 1

Crystallographic experimental details. Experiments were carried out at 100 K with graphite monochromated Mo K α radiation on Bruker AXS SMART APEX CCD or APEX-II CCD diffractometers.

	LH	1 = $(\text{LH})_3\text{ZnBr}_2$	2 = $(\text{LH})_3\text{CoCl}_2$	3 = $(\text{LH})_4\text{MnCl}_2$	4 _{EtOH} = $(\text{LH})_4\text{NiBr}_2 \cdot \text{EtOH}$
Chemical formula	$\text{C}_8\text{H}_{15}\text{N}_3$	$\text{C}_{24}\text{H}_{45}\text{Br}_2\text{N}_9\text{Zn}$	$\text{C}_{24}\text{H}_{45}\text{ClCoN}_9\text{Cl}$	$\text{C}_{32}\text{H}_{60}\text{ClMnN}_{12}\text{Cl}$	$\text{C}_{32}\text{H}_{60}\text{Br}_2\text{N}_{12}\text{Ni} \cdot \text{C}_2\text{H}_6\text{O}$
M_r	153.23	684.88	589.52	738.76	877.51
Crystal system, space group	monoclinic, $P2_1/c$	trigonal, $R3c:H$	monoclinic, $P2_1/c$	triclinic, $P\bar{1}$	monoclinic, $P2_1/n$
a, b, c (Å)	9.030 (5), 10.662 (7), 18.516 (11)	13.850 (3), 13.850, 27.831 (7)	9.1109 (12), 28.167 (4), 12.1977 (16)	12.4871 (6), 12.4903 (6), 14.1462 (7)	11.9812 (9), 29.808 (2), 12.0344 (10)
α, β, γ (°)	90, 91.78 (2), 90	90, 90, 120	90, 101.607 (2), 90	72.856 (3), 78.438 (3), 89.997 (3)	90, 90.316 (2), 90
V (Å ³)	1781.7 (19)	4623 (3)	3066.2 (7)	2061.42 (18)	4297.8 (6)
Z	8	6	4	2	4
μ (mm ⁻¹)	0.07	3.42	0.76	0.49	2.35
Crystal shape	rod	block	plate	plate	block
Colour	colourless	colourless	green	colourless	green
Crystal size (mm)	$0.44 \times 0.20 \times 0.10$	$0.41 \times 0.21 \times 0.18$	$0.35 \times 0.16 \times 0.08$	$0.27 \times 0.26 \times 0.04$	$0.55 \times 0.55 \times 0.38$
Absorption correction	Multi-scan, Apex2	Multi-scan, Apex2	Multi-scan, Apex2	Multi-scan, TWINABS	Multi-scan, Apex2
$T_{\text{minimum}}, T_{\text{maximum}}$	0.648, 0.746	0.581, 0.746	0.616, 0.746	0.565, 0.746	0.523, 0.746
No. of meas., indep., obs. [$I > 2\sigma(I)$] refl.	8728, 4352, 2771	7226, 2636, 2093	25275, 9132, 6893	12873, 12873, 8614	100363, 13513, 10798
R_{int}	0.046	0.031	0.037	0.0859	0.042
$(\sin \theta/\lambda)_{\text{max}}$ (Å ⁻¹)	0.667	0.719	0.730	0.741	0.739
Range of h, k, l	$h = -11 \rightarrow 12, k = -14 \rightarrow 13, l = -24 \rightarrow 20$	$h = -19 \rightarrow 14, k = -5 \rightarrow 19, l = -25 \rightarrow 39$	$h = -13 \rightarrow 13, k = -40 \rightarrow 39, l = -17 \rightarrow 14$	$h = -17 \rightarrow 18, k = -17 \rightarrow 18, l = 0 \rightarrow 20$	$h = -17 \rightarrow 17, k = -43 \rightarrow 43, l = -17 \rightarrow 17$
$R[F^2 > 2\sigma(F^2)], wR(F^2), S$	0.059, 0.148, 1.01	0.025, 0.065, 1.05	0.042, 0.106, 1.03	0.056, 0.132, 1.02	0.042, 0.103, 1.08
No. reflections, parameters, restraints	4352, 219, 4	2636, 114, 1	9132, 365, 14	12,873, 454, 6	13,513, 773, 277
$\Delta\rho_{\text{maximum}}, \Delta\rho_{\text{minimum}}$ (e Å ⁻³)	0.28, -0.26	0.44, -0.32	0.76, -0.46	0.57, -0.55	1.58, -0.76

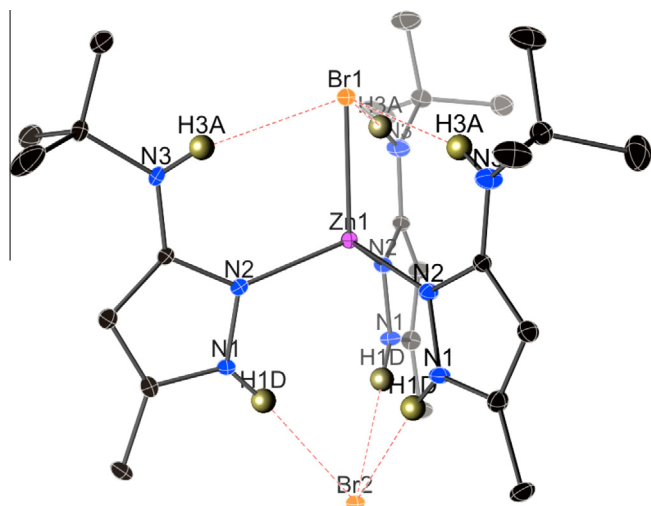


Fig. 2. Structural diagram for $(\text{LH})_3\text{ZnBr}_2$ (**1**). Ellipsoids are shown at 30% probability. Hydrogen bonds are shown with red dashed lines. Non-hydrogen bonding hydrogens are omitted for clarity. (Colour online.)

(nearly) octahedral geometry. Regardless of the metal to ligand ratio used in the synthesis the same complex is formed. For example, the $(\text{LH})_4\text{NiBr}_2$ product is formed from a three to one ratio of ligand to metal with some unreacted metal salt leftover in this case. These crystal structures are described below. The metal complexes (**1–3**) made from LH show hydrogen bonding interactions that are summarized and compared in Table 3; the influence of the geometry on the strength of the hydrogen bonds and the M–X distances is readily apparent and is discussed below.

2.2. Crystal Structures

The pyrazole ligand is a known compound but the X-ray crystal structure shown in Fig. 1 is new. The crystallographic experimental data for this compound and all other compounds is given in Table 1. 3-NH-*t*-Butyl-5-methyl-pyrazole (LH) shows a network of hydrogen bonds that connect four pyrazole molecules in the crystal phase (Fig. 1). Two LH molecules are in the asymmetric unit,

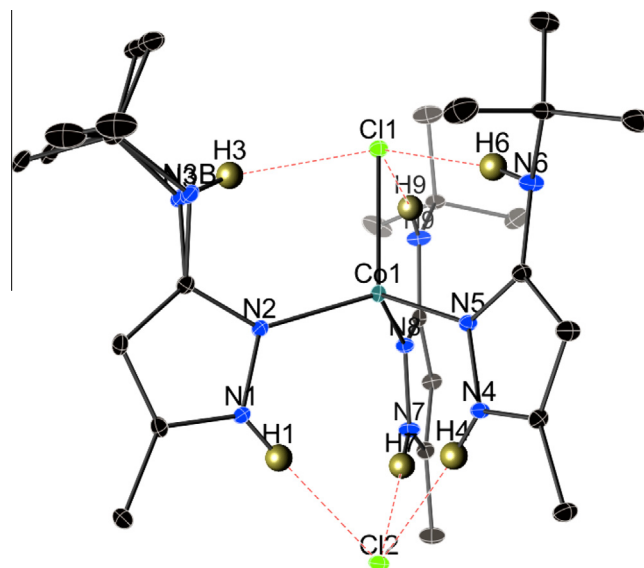
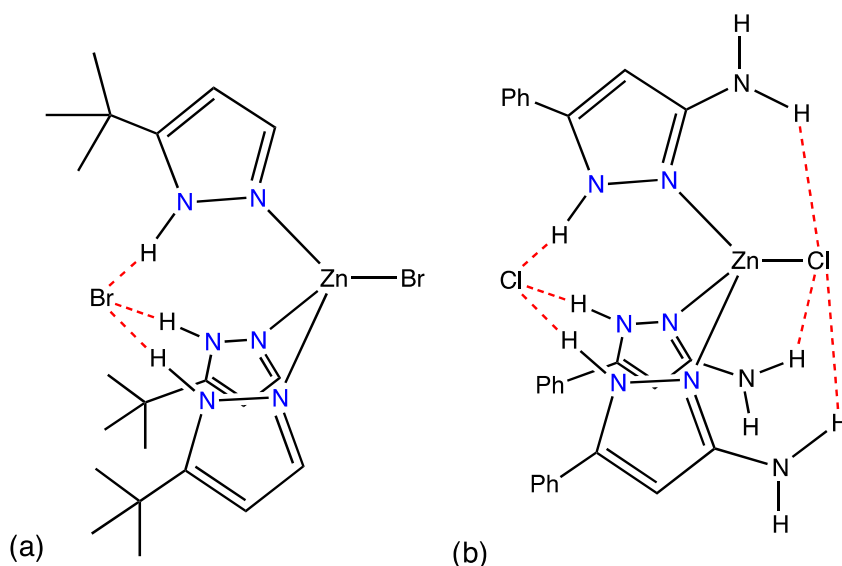


Fig. 3. Structural diagram for $(\text{LH})_3\text{CoCl}_2$ (**2**). Ellipsoids are shown at 30% probability. Hydrogen bonds are shown with red dashed lines. Non-hydrogen bonding hydrogens are omitted for clarity. The pyrazole ring on the left shows disorder in the NH-*t*-Bu unit. (Colour online.)

and eight LH molecules are in the unit cell. Each pyrazole moiety shows three hydrogen bonds to neighboring pyrazole molecules in the crystal phase. There are six weak [32] N–H···N hydrogen bonds in this structure (all N···N distances are above 2.914(3) Å); N–H1 and N–H3 are hydrogen bond donors and N2 is a hydrogen bond acceptor. However, as shown below, N2 can also bind to a metal.

The zinc complex with 3-(NH-*t*-butyl)-5-methyl-pyrazole (LH), Fig. 2, binds two bromide ions forming a ditopic salt with the formula $(\text{LH})_3\text{ZnBr}_2$ (**1**). One bromide (Br1) is bound by Zn and three weak hydrogen bonds (N···Br = 3.441(3) Å, N–H···Br = 161.9(2)°) [33]. The other bromide (Br2) is bound by three moderate strength hydrogen bonds [33] (N···Br = 3.281(3) Å, N–H···Br = 173.6(2)°); Table 3 shows that the moderate strength hydrogen bonds exhibit N···Br distances that are less than the distance predicted from the ionic radius of bromide and the covalent radii of N and H



Scheme 4. The closest literature analogs to our complexes **1–4** are (a) (3-*t*-butyl-pyrazole)₃ZnBr₂ [34] and (b) (3-amino-5-phenyl-pyrazole)₃ZnCl₂ [35]. These structures show intramolecular hydrogen bonds.

atoms. Notably, this structure is dominated by intramolecular hydrogen bonds, and intermolecular hydrogen bonds are not present in the crystal phase. A close analog to this structure in the literature is (3-*t*-butyl-pyrazole)₃ZnBr₂ (Scheme 4a) in which three hydrogen bonds encapsulate a halide ion [34]; interestingly this complex has the *t*-butyl groups turned away from the metal center unlike the arrangement seen for **1**. Also similar to **1** is the reported structure of (3-amino-5-phenyl-pyrazole)₃ZnCl₂ (Scheme 4b) which also features N–H to Cl hydrogen bonding interactions [35]. Halides seem especially well suited for hydrogen bonding in this geometry as, notably, some Zn(II) complexes of 3-amino substituted pyrazole ligands that lack halides do not exhibit such hydrogen bonding arrangements [36,37]. The Zn–Br distance in **1** is very long, at 2.441(1) Å (cf. Zn–Br = 2.3557(3) Å in (3-*t*-butyl-pyrazole)₃ZnBr₂ [34] and 2.399 Å defines the start of the upper quartile for four coordinate Zn–Br bond distances in Orpen's review [38]). However, a Zn–Br bonding interaction is still present in **1** as shown by a distance that is less than 2.56 Å, which is the sum of the ionic radii for Zn^{II} and bromide (Table 3). The Zn–Br bond lengthening (relative to average Zn–Br distances) is a result of three weak hydrogen bonds. Interestingly, the structure in Fig. 2 resembles a scorpionate complex, but the ligands are tethered by three hydrogen bonds to a halide rather than three covalent bonds.

Similarly, the cobalt complex, (LH)₃CoCl₂ (**2**) (Fig. 3), shows six hydrogen bonds that bind two chloride anions. Again, there are strong hydrogen bonds (ranging from 3.122(2) to 3.132(2) Å for N to Cl₂ distances with nearly linear angles ranging from 175.5(1) to 178.6(1)° away from the metal and weak hydrogen bonds near the metal (3.318(2) to 3.338(3) Å for N to Cl₁ distances, and 164(2) to 170(2)° for N–H...Cl angles). The Co–Cl₁ distance is relatively long (at 2.302(1) Å), indicating that the three hydrogen bonds have weakened the chloride to metal interaction [38]. Like the zinc complex (Fig. 2), the cobalt complex in Fig. 3 resembles a scorpionate complex but is held together by the ligand to metal interactions and hydrogen bonds. As shown in Tables 2 and 3, complexes **1** and **2** have very similar metrical parameters (especially when compared to the calculated values) and both indicate hydrogen bonds that weaken somewhat the M–X bond.

In contrast, the manganese complex, (LH)₄MnCl₂ (**3**) (Fig. 4), has a ligand to metal ratio of 4:1. This arrangement appears to make the hydrogen bonds weaker with N to Cl₂ distances ranging from 3.114(3) Å to 3.128(3) Å with N–H...Cl₂ angles 137.0(2)–138.2

(2)° in the empty cavity above the metal. Given the structure type (which constrains N to Cl distances) the angles are a better measure of hydrogen bond strength than the distances [32]. The Mn–Cl₁ bond and the Mn to Cl₂ ionic interaction forces the chlorides to be close to the NH of the pyrazole co-ligands regardless of whether (or not) hydrogen bonds are present. Thus, these non-linear angles (Table 3) indicate very weak hydrogen bonds are present. Around the Mn–Cl₁ bond, the hydrogen bonds appear more linear with N–H...Cl₁ angles of 167(3)–171(3)° but N to Cl₁ distances are longer and range from 3.306(3) Å to 3.320(3) Å. Through comparison with the cobalt structure (Fig. 3), it appears that a 4:1 ratio of ligand to metal leaves the hydrogen bonds around the M–Cl bond relatively unperturbed (which use NH-*t*-butyl), but the hydrogen bonds from the NH of the pyrazole ring are much weaker due to angle deviations. The Mn–Cl₁ distance is 2.470(1) Å, a value that is much longer than typical Mn–Cl distances for five coordinate complexes (2.358 Å marks the 75th percentile for Mn–Cl distances [38] and 2.47 Å is the sum of the ionic radii for Mn^{II} and chloride). This Mn–Cl₁ bond lengthening could be due to the NH hydrogen bonds or due to a weak Mn–Cl₂ ionic interaction (2.954(1) Å shows a short contact but not a bond).

Unlike complexes **1–3**, the nickel complex, (LH)₄NiBr₂ (**4**) (Fig. 5), does not show any NH to Br hydrogen bonds. Complexes **1–3** lack solvent molecules in the crystal phase, but complex **4** contains ethanol solvent in the structure. In **4**, the N...Br distances are too long (3.336(4)–3.454(2) Å) for hydrogen bonding interactions, and the N–H...Br angles are non-linear (Table 3). Furthermore, the pyrazole rings are tilted at an angle (relative to the Ni–Br axis with Br–Ni–N–(C/N) torsion angles of 36–46°) forcing the NH groups to tilt away from the bromides. In contrast, analogous halide–M–N–(C/N) torsion angles are ~11–16° for the Mn complex **3**, ~0–7° for the Co complex **2**, and ~1° for the Zn complex **1**. Thus, (LH)₄NiBr₂ is the first complex in this series to show the pyrazole rings canted (relative to the Br–Ni–Br axis) since the NH to halide hydrogen bonding interaction is not present. The presence of disordered ethanol solvent (not shown in Fig. 5) which hydrogen bonds to bromide (Br₂) in the crystal phase likely explains why this structure lacks NH to bromide hydrogen bonds. This interaction likely explains why the Ni₁ to Br₂ distance is so long; at 2.809(1) Å it is well above the 75th percentile value of 2.572 Å [38]. The Ni₁ to Br₁ distance is more typical at 2.568(1) Å, which is less than the sum of the ionic radii (2.65 Å). This is the only structure that shows two M–X bonds, although one is weak.

Table 2

Bond lengths (Å) and angles (°) for complexes **1–4**. Complex **1** displays C₃ symmetry and thus there are only 2 unique bond lengths and angles around the metal center. Comparable distances are shown in grey.

1 = (LH) ₃ ZnBr ₂	2 = (LH) ₃ CoCl ₂	3 = (LH) ₄ MnCl ₂	4 _{EtOH} = (LH) ₄ NiBr ₂ ·EtOH
Zn1-Br1 2.411(1)	Co1-Cl1 2.302(1)	Mn1-Cl1 2.470(1)	Ni1-Br1 2.568(1)
	Co1-N2 2.011(2)	Mn1-N2 2.263(3)	Ni1-Br2 2.809(1)
	Co1-N5 2.012(2)	Mn1-N5 2.264(3)	Ni1-N2 2.092(2)
	Co1-N8 2.000(2)	Mn1-N8 2.269(3)	Ni1-N5 2.093(2)
		Mn1-N11 2.264(3)	Ni1-N8 2.087(2)
Zn1-N2 2.023(3)	Co1-N _{avg} 2.008(2)	Mn1-N _{avg} 2.265(2)	Ni1-N11 2.086(2)
	Cl1-Co1-N2 108.2(1)	Cl1-Mn1-N2 97.5(1)	Ni1-N _{avg} 2.090(1)
	Cl1-Co1-N5 108.5(1)	Cl1-Mn1-N5 96.6(1)	Br1-Ni1-N2 92.5(1)
	Cl1-Co1-N8 106.9(1)	Cl1-Mn1-N8 96.7(1)	Br1-Ni1-N5 92.9(1)
		Cl1-Mn1-N11 96.2(1)	Br1-Ni1-N8 92.8(1)
Br1-Zn1-N2 110.2(1)	Cl1-Co1-N _{avg} 107.9(1)	Cl1-Mn1-N _{avg} 96.7(1)	Br1-Ni1-N11 93.1(1)
			Br1-Ni1-N _{avg} 92.8(1)
	N2-Co1-N5 108.4(1)	N2-Mn1-N5 89.4(1)	Br2-Ni1-N _{avg} 87.2(1)
	N2-Co1-N8 112.0(1)	N2-Mn1-N11 89.4(1)	N2-Ni1-N5 89.4(1)
	N5-Co1-N8 112.7(1)	N5-Mn1-N8 89.1(1)	N2-Ni1-N11 90.4(1)
		N8-Mn1-N11 89.0(1)	N5-Ni1-N8 89.8(1)
N2-Zn1-N2 108.8(1)	N-Co1-N _{avg} 111.0(1)	<i>cis</i> N-Mn-N _{avg} 89.2(1)	N8-Ni1-N11 89.9(1)
		<i>trans</i> N-Mn-N _{avg} 166.5(1)	<i>cis</i> N-Ni-N _{avg} 89.9(1)
			<i>trans</i> N-Ni-N _{avg} 174.3(1)

Table 3
A comparison of bond lengths and angles relevant to hydrogen bonding in complexes **1–4**. Nearly linear N–H–X angles are an indication of strong hydrogen bonding interactions [32]. The directly comparable data is shaded in the same colour for ease of comparison of experimental and calculated data.

	1	2	3	4 _{EtOH}
<i>Experimental data</i>				
M:LH ratio	3	3	4	4
M–X1 (Å)	2.441(1) (Zn–Br)	2.302(1) (Co–Cl)	2.470(1) (Mn–Cl)	2.568(1) (Ni–Br)
M–X2 (Å)	4.523(2) (Zn–Br)	4.190(1) (Co–Cl)	2.954(1) (Mn–Cl)	2.809(1) (Ni–Br)
X···N (Å)	non-bonded 3.281(3) 3.441(3) (Br···N)	non-bonded 3.122(2)–3.132(2) 3.318(2)–3.338(3) (Cl···N)	non-bonded 3.114(3)–3.128(3) 3.306(3)–3.320(3) (Cl···N)	weak bonded 3.336(4)–3.454(2) (Br···N)
N–H–X angle (°)	173.6(2) 161.9(2) (N–H–Br)	175.5(1)–178.6(1) 164(2)–170(2) (N–H–Cl)	137.0(2)–138.2(2) 167(3)–171(3) (N–H–Cl)	113(3)–146(3) (N–H–Br)
<i>Calculated data</i>				
$r_{\text{ionic}}(\text{M}) + r_{\text{ionic}}(\text{X})$ (Å) ^a	2.56 (Zn–Br)	2.39 (Co–Cl)	2.47 (Mn–Cl)	2.65 (Ni–Br)
$r_{\text{cov}}(\text{N}) + 2 r_{\text{cov}}(\text{H}) + r_{\text{ionic}}(\text{X})$ (Å) ^b	3.31 (N···Br _{min} via N–H···Br)	3.16 (N···Cl _{min} via N–H···Cl)	3.16 (N···Cl _{min} via N–H···Cl)	3.31 (N···Br _{min} via N–H···Br)

^aThe calculated values of M–X come from the ionic radii of the bound ions to estimate M–X distances as the sum of the ionic radii. A significant bonding interaction should decrease this distance. Conversely, hydrogen bonding to the halide can lengthen this distance.

^bThe minimal N–X distance involving a hydrogen bonded (NH···X) interaction, as calculated from the covalent and ionic radii of the atoms (N, H) and ions (X = Cl[−] or Br[−]) involved in hydrogen bonding.

2.3. Mass spectrometry (MS)

The strength of the hydrogen bonds for **1** and **2** is reflected by the MS results. Complex **1** is stable enough to be detected in the mass spectrometer, reflecting the strength and persistence of the bonds in the complex. Therefore, the complex is effective at anion binding, as shown here with bromide. Other examples of anion binding through hydrogen bonds have been reported in the literature [39–43]. Complex **2** is also relatively stable in the mass spectrometer, with the loss of an HCl unit occurring before it reaches the detector and the observed ion corresponds to [(LH)₂(L)CoCl]⁺. For complex **3**, the relative weakness of hydrogen bonds and metal to pyrazole interactions is shown by the loss of L and Cl prior to reaching the detector with the FAB MS method, and the loss of

one pyrazole ring (LH) when using the softer LIFDI method. Similar to the manganese complex **3**, the relatively weak interactions in **4** are shown by loss of LH and bromide by the FAB MS technique, and the loss of LH in the highest molecular weight peak when using the softer LIFDI technique.

2.4. Spectroscopy

Complexes **1–4** present two distinct structure types – (LH)₄MX₂ (Ni and Mn) and (LH)₃MX₂ (Co and Zn). We will discuss the structure types independently, focusing on the more spectroscopically accessible Ni and Co complexes. The d⁵ Mn(II) ion gives very weak optical spectra, and its electron relaxation properties generally make ¹H NMR unobservable. Consequently, its complexes can only

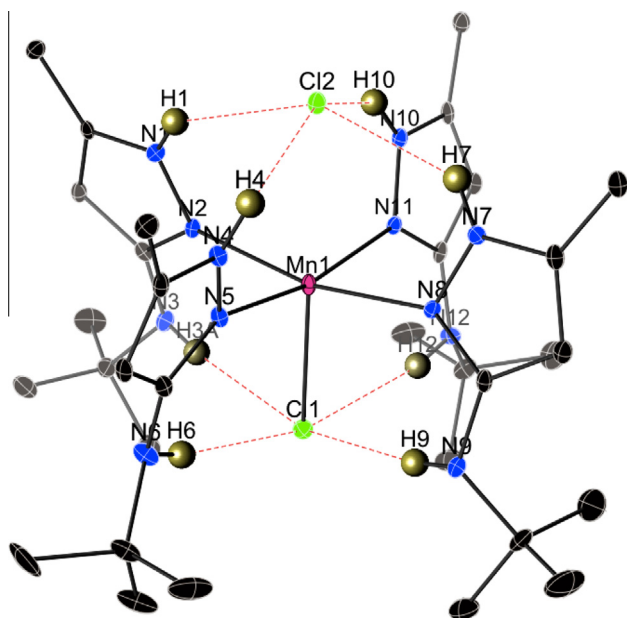


Fig. 4. Structural diagram for (LH)₄MnCl₂ (**3**). Ellipsoids are shown at 30% probability. Hydrogen bonds are shown with red dashed lines. Non-hydrogen bonding hydrogens are omitted for clarity. (Colour online.)

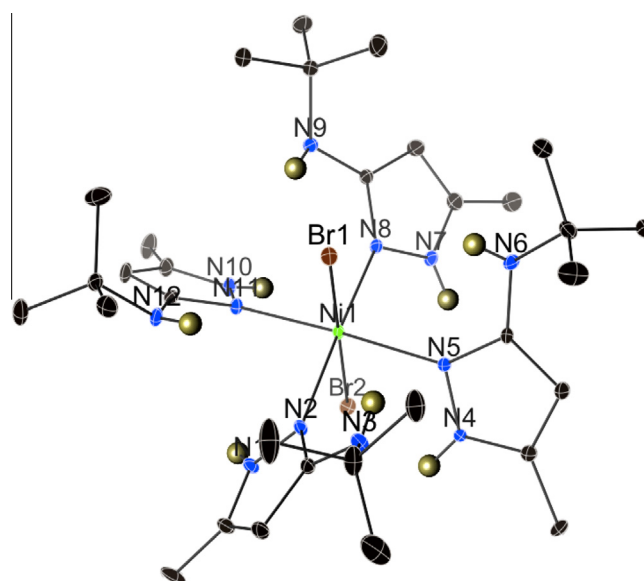


Fig. 5. Structural diagram for (LH)₄NiBr₂ (**4**). Ellipsoids are shown at 30% probability. Most hydrogens and ethanol solvent molecule are omitted for clarity. Disordered atoms have been hidden for clarity, see the Supporting Information for a view that includes disordered ethanol and pyrazole rings.

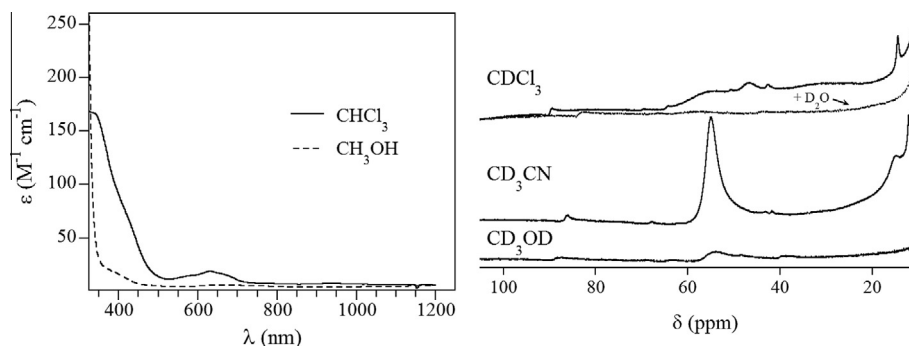


Fig. 6. (left) UV-vis-NIR spectra in CHCl_3 (solid line) and CH_3OH (dashed line) and (right) 200 MHz ^1H NMR of $(\text{LH})_4\text{NiBr}_2$ (**4**) in different solvents.

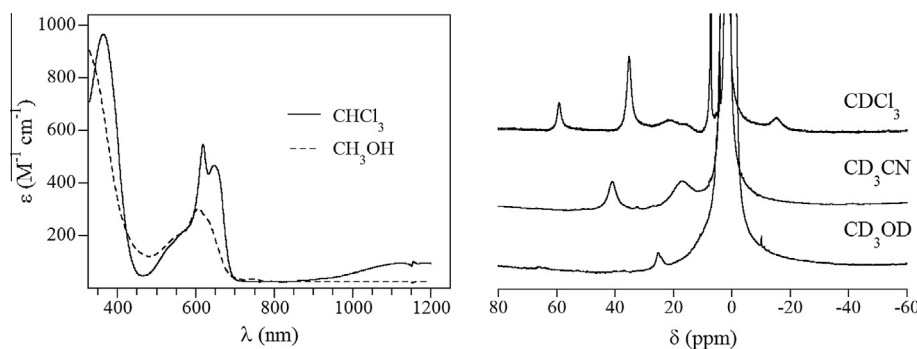


Fig. 7. UV-vis-NIR (left) and 200 MHz ^1H NMR in CDCl_3 (right) of $(\text{LH})_3\text{CoCl}_2$ (**2**).

be probed using EPR. Similarly, the d^{10} Zn(II) ion is neither optically nor EPR active, and its complexes give NMR spectra that are often difficult to distinguish from those of the uncomplexed ligand. In contrast, the d^8 Ni(II) ion gives meaningful optical spectra and its complexes are amenable to NMR, while complexes of the d^7 Co(II) ion give readily observable signals in optical, NMR and EPR spectroscopies.

As discussed above, the two $(\text{LH})_4\text{MX}_2$ complexes yielded different crystal structures, dependent on the presence, or absence, of a hydrogen-bonding solvent in the crystal lattice. To determine if these two substructures could interconvert, we examined the solvent-dependence of their spectroscopy. The optical spectrum of $(\text{LH})_4\text{NiBr}_2$ (**4**) in chloroform shows a strong $\text{Br} \rightarrow \text{Ni}$ CT band and weak, but measurable ligand-field intensity (Fig. 6, left). Although not conclusive, the ligand-field extinction coefficients are consistent with previously reported five-coordinate Ni(II) Tp complexes [44,45] and larger than expected for a six-coordinate Ni(II) [46]. The CT band shifts to much higher energy in methanol, and the ligand-field bands are almost entirely attenuated, suggesting the H-bonding solvent alters, or possibly disrupts the structure of the complex. ^1H NMR of the Ni(II) complex is also highly solvent-dependent (Fig. 6, right). In CDCl_3 , the Ni(II) complex gives a very broad envelope of resonances from 15 to 65 ppm, all of which virtually disappear on introduction of 20 μl of D_2O (and are nearly absent in CD_3OD). In CD_3CN , the ^1H NMR spectrum sharpens significantly, accompanied by small changes in chemical shift. This may reflect replacement of one or both bromide ions with coordinated acetonitrile, or it may reflect the conversion of (**4**) into the H-bonded structure demonstrated by the Mn(II) complex. We were unable to examine the temperature-dependence of the Ni(II) complex's NMR, due to significant precipitation at lower temperatures. EPR of the Mn complex (**3**) (Fig. S10) in 70/30 toluene/chloroform (aprotic, non-coordinating solvents) shows a common 6-line

pattern at $g = 2.0$ ($A(^{55}\text{Mn}) = 82$ G), and lower-field transitions, consistent with the outer doublets of an $S = 5/2$ Mn(II) ion under the influence of a small zero-field splitting ($D \sim 0.1$ cm^{-1}) [47]. These values of g , A , and D are similar to well-characterized octahedral complexes of Mn(II), including MnN_4Cl_2 complexes [48], suggesting the Mn(II) complex may be six-coordinate in frozen solution, with the possible coordination of chloride in the sixth site. Although poorly resolved, ^{14}N hyperfine couplings clearly indicate that the pyrazole ligands remain coordinated. However, at present, it is difficult to determine if the Mn(II) complex retains the five-coordinate structure seen in the crystal structure in solution, or collapses to the canted structure shown by the Ni(II) complex. Overall, the spectroscopy is consistent with intact Ni(II) and Mn(II) complexes in both aprotic and protic solvents, and leaves open the possibility that these structures will interconvert, dependent on the properties of the solvent.

The Co(II) complex, $(\text{LH})_3\text{CoCl}_2$, representing the other structure type, shows similar solvent dependence, with protic solvents appearing to disrupt the structure. In chloroform, the Co(II) complex (**2**) shows a strong $\text{Cl} \rightarrow \text{Co}$ CT band at $\lambda \sim 390$ nm and ligand-field transitions that extend from $\lambda \sim 475$ to 700 nm, along with a weaker ligand-field transition near 1100 nm (Fig. 7, left), and extinction coefficients consistent with four coordination. The CT band shifts to higher energy in methanol, and the intensity in the ligand-field region is dramatically attenuated, suggesting the hydrogen-bonding solvent may either alter the structure of the complex itself, or alter the hydrogen-bonding interaction with the halide ion. Conversion to a higher-coordination $\text{CoCl}_x(\text{LH})_y(\text{MeOH})_z$ complex would also allow for retention of the $\text{Cl} \rightarrow \text{Co}$ CT band and account for attenuated ligand-field transitions. Proton NMR in CDCl_3 shows sharp features that are consistent with retention of the H-bonded structure (Fig. 7, right), and temperature-dependent studies (Fig. S7) show evidence of

dynamic behavior, including coalescence of a the pair of peaks near 20 ppm (most likely from the *t*-butyl groups) at low temperature, and a sharp-to-broad-to-sharp pattern displayed by the most downfield shifted resonance. While the nature of these dynamics is at present unclear, and is the subject of further study, the temperature-dependent ^1H NMR of the Co^{II} complex clearly indicates that the complex remains intact in CDCl_3 , and that it is in motion. EPR of the Co^{II} complex further supports its description as an intact tetrahedral complex based on weak intensity and its line shape (Fig. S8) [49]. The ^1H NMR spectrum of the Zn^{II} complex (**1**) in CDCl_3 (Fig. S1) shows only resonances attributable to an intact cluster, including a very broad solvent exchangeable resonance. Overall, spectroscopy of the $(\text{LH})_3\text{MX}_2$ complexes suggests that indeed the two structure types may interconvert.

3. Conclusions

The complexes described herein are composed of “scorpionate like” chelates in which the chelating ligand (which is composed of three or four 3-NH(*t*-butyl)-5-methyl-pyrazole molecules) is held together by hydrogen bonds. Thus, complexes **1**, **2**, and **3** have NH to halide hydrogen bonds that support a structure with pyrazole to metal ratios of 3:1 or 4:1. In contrast, intramolecular hydrogen bonds are absent from **4**, the 4:1 nickel complex with the same pyrazole ligand. However, this may be due to ethanol solvent being present for **4**. These hydrogen-bonded self-assembled structures hold together in the solid state and in relatively non-polar solutions (e.g. chloroform). However, spectroscopic studies in methanol suggest that these scorpionate-like hydrogen bonded complexes are disrupted in polar solution, presumably because hydrogen bonds to solvent can replace the intramolecular hydrogen bonds. These complexes could be applied towards the development of sensors for halide ions in organic solutions, whereby the binding of halide ions could be detected by changes in the UV-Visible spectral features [50]. Furthermore, this pyrazole ligand shows an ability to form hydrogen bonds to anions that in some ways resemble anion-binding catalysis in synthetic systems [51,52] and in natural enzymes [53].

4. Experimental

4.1. General

All commercially available reagents were used as received. The reactions to form **1–4** were generally not air sensitive and reactions were run both in air and under nitrogen giving identical results, and most purification and isolation procedures were done open to air. Anhydrous MX_2 salts were weighed out in a glovebox to prevent moisture absorption so an accurate mass could be obtained. Organic solvents were used as received. Proton and carbon NMR spectra were recorded using either a 300 MHz (^1H NMR spectra, 75 MHz for ^{13}C NMR spectra on this instrument) or a 500 MHz (used primarily for ^1H NMR) Varian Unity Inova NMR spectrophotometer at Drexel University. ^1H NMR spectroscopy experiments were also done at Miami University on a 200 MHz NMR instrument. Infrared spectra were collected on a Perkin Elmer Spectrum One FT-IR spectrometer using a universal ATR sampling accessory. High resolution (HR) mass spectrometry was performed on a VG70SE double focusing, triple quadrupole mass spectrometer equipped with FAB or CI ionization capability. Electrospray ionization (ESI) mass spectrometry was performed on a SCIEX API3000 mass spectrometer for fast atom bombardment (FAB, cesium ion). Elemental analysis was performed by Robertson Microlit, Ledgewood, NJ.

4.2. Synthesis of 3-NH(*t*-butyl)-5-methyl-pyrazole (LH)

This compound was synthesized according to a literature procedure [21].

4.3. Synthesis of $(\text{LH})_3\text{ZnBr}_2$ (**1**)

The pyrazole LH (1.001 g, 6.533 mmol) was treated with ZnBr_2 (0.491 g, 2.18 mmol) in 50 mL of ethanol and allowed to stir for 20–24 h. Then, the solvent was removed under vacuum to produce a yellow oil. The product was recrystallized from CH_2Cl_2 and pentane (1:2) which allowed for the isolation of a crystalline precipitate (95% yield, 1.418 g, 2.071 mmol) that was dried under vacuum. ^1H NMR in CDCl_3 (δ , ppm): 1.293 (tBu, s, 27H), 2.266 (Me, s, 9H), 5.569 (4-pz, s, 3H). ^{13}C NMR in CDCl_3 (δ , ppm): 11.74 (Me), 29.71 ($\text{C}(\text{CH}_3)_3$), 51.59 ($\text{C}(\text{CH}_3)_3$), 93.39 (4-pz), 144.22 and 155.63 (3-pz and 5-pz). IR (ν , cm^{-1}): 3370, 3151, 3082, 2978, 2877, 1585, 1514, 1397, 1367, 1230, 1212, 1040, 957, 774. FAB MS (m/z): 684.1 [M] $^+$, 604.2 [$\text{M}-\text{HBr}$] $^+$, 451.1 [$\text{M}-\text{HBr}-\text{LH}$] $^+$, 298.0 [$\text{M}-\text{HBr}-2\text{LH}$] $^+$. High res. MS: (m/z) = 602.2297 expt. (602.2273 calcd.), 604.2234 expt. (604.2252 calcd.). In both MS experiments, all peaks showed the expected isotopic pattern. Elemental Anal. expt. Calcd.: C, 43.04 (42.09); H, 6.74 (6.62); N, 18.57 (18.41).

4.4. Synthesis of $(\text{LH})_3\text{CoCl}_2$ (**2**)

The pyrazole LH (0.100 g, 0.653 mmol) was treated with CoCl_2 (0.028 g, 0.22 mmol) in 5 mL of ethanol and allowed to stir for 3 days. Then, the solvent was removed under vacuum to produce a solid. The product was recrystallized from the diffusion of hexanes into a methanol solution using the vapor diffusion recrystallization technique. The crystalline product was formed in 96% yield (0.122 g, 0.207 mmol) and was dried under vacuum. IR (ν , cm^{-1}): 3362, 3350, 3326, 3153, 3045, 2968, 2923, 2873, 1652, 1589, 1549, 1515, 1400, 1366, 1298, 1228, 1211, 1141, 1040, 956, 776, 749. FAB MS (m/z): 553.3 [$\text{M}-\text{HCl}$] $^+$, 400.2 [$\text{M}-\text{HCl}-\text{LH}$] $^+$, 247.0 [$\text{M}-\text{HCl}-2\text{LH}$] $^+$; all peaks showed the expected isotopic pattern. High res. MS: (m/z) = 553.2816 expt. (553.2818 calcd.); the expected isotopic pattern was observed. Elemental Anal. expt. Calcd.: C, 49.03 (48.90); H, 7.80 (7.69); N, 21.34 (21.38).

4.5. Synthesis of $(\text{LH})_4\text{MnCl}_2$ (**3**)

The pyrazole LH (0.100 g, 0.653 mmol) was treated with MnCl_2 (0.020 g, 0.16 mmol) in 5 mL of ethanol and allowed to stir for 3 days. Then, the solvent was removed under vacuum to produce a solid. The product was recrystallized from CH_2Cl_2 and hexanes (3:1) which allowed for the isolation of a crystalline precipitate (96% yield, 0.114 g, 0.154 mmol) that was dried under vacuum. IR (ν , cm^{-1}): 3320, 2971, 1576, 1539, 1512, 1393, 1362, 1289, 1233, 1150, 1017, 956, 809, 747, 662. FAB MS (m/z): 550.1 (weak) [$\text{M}-\text{L}-\text{Cl}$] $^+$, this complex fragments quickly in the MS and all other peaks are LH or a dimer or trimer of LH; all peaks showed the expected isotopic pattern. High res. MS: (m/z) = 551.3024 expt. (551.3023 calcd.) [$\text{M}+\text{H}-\text{L}-\text{Cl}$] $^+$; these and other peaks showed the expected isotopic pattern. Due to fast fragmentation and loss of one L prior to reaching the detector, we also studied this compound by LIFDI MS, which is a softer technique but we saw similar results: (m/z) = 584 [$\text{M}-\text{LH}$] $^+$, 549 [$\text{M}-\text{LH}-\text{Cl}$] $^+$, 431 [$\text{M}-2\text{LH}$] $^+$.

4.6. Synthesis of $(\text{LH})_4\text{NiBr}_2$ (**4**)

The pyrazole LH (0.200 g, 1.31 mmol) was treated with NiBr_2 (0.071 g, 0.33 mmol) in 10 mL of ethanol and allowed to stir for 2 days. Then, the solvent was removed under vacuum to produce a solid. The product was recrystallized from ethanol which allowed

for the isolation of a crystalline precipitate (67% yield, 0.181 g, 0.218 mmol) that was dried under vacuum. The structure is $(\text{LH})_4\text{NiBr}_2$ when rigorously dried under vacuum, although $[(\text{LH})_4\text{NiBr}_2]\text{EtOH}$ is observed crystallographically. IR (ν , cm^{-1}): 3315, 2972, 2930, 1579, 1508, 1393, 1361, 1238, 1025, 739. FAB MS (m/z): 598.4 $[\text{M}-\text{LH}-\text{HBr}]^+$, 445.2 $[\text{M}-2\text{LH}-\text{HBr}]^+$; all peaks showed the expected isotopic pattern. Due to fast fragmentation and loss of one L prior to reaching the detector, we also studied this compound by LIFDI MS, which is a softer technique but we saw similar results: (m/z) = 678 $[\text{M}-\text{LH}]^+$, 598 $[\text{M}-\text{LH}-\text{HBr}]^+$, 524 $[\text{M}-2\text{LH}-\text{H}]^+$, 445 $[\text{M}-2\text{LH}-\text{HBr}]^+$.

4.7. NMR Spectroscopy

Proton NMR spectra were obtained on a Bruker ASX200 NMR spectrometer, from 5 mM solutions, maintaining temperature with the temperature-controller, heater and thermocouple provided with the instrument. For the Co(II) complex, each spectrum consisted of 1000 transients of 4 k data points over a 75 kHz (375 ppm) spectral window ($t_{\text{AQ}} \sim 55$ ms), employing a 4 μs excitation pulse. For the Ni(II) complex, 1000 transients of 8 k data points were collected over the same 75 kHz spectral window ($t_{\text{AQ}} \sim 110$ ms). For the Zn(II) complex, 128 transients of 16 k data points were collected over a 4 kHz (20 ppm) spectral window ($t_{\text{AQ}} \sim 1.2$ s). Prior to Fourier transformation, all FIDs were apodized using an exponential function that introduced an additional line width of 10 Hz (0.05 ppm).

4.8. EPR Spectroscopy

Frozen solution (~ 2 mM) X-band EPR spectra were recorded on a Bruker EMX EPR spectrometer equipped with an ER-4116DM dual mode resonator, with temperature maintained by an Oxford ESR900 flow cryostat. All samples were approximately 2 mM in concentration, and thoroughly degassed by multiple freeze-pump-thaw cycles prior to data collection. The spectra presented herein were recorded using the following conditions: $T = 4.5$ K, $n_{\text{MW}} = 9.62$ GHz (0.2 mW); 10 G field modulation (100 kHz); receiver gain = 10^4 ; time constant = 41 ms.

4.9. Single crystal X-ray diffraction

Crystallographic structure determinations were performed on single crystals of LH, **1**, **2**, **3** and **4**_{EtOH}. Experimental details are provided in the [Supporting Information](#).

Acknowledgements

We thank Eric J. Schelter, Robert C. Scarrow, and Deidra L. Gerlach for helpful suggestions. We thank NSF CAREER (Grant CHE-0846383 and CHE-1360802 to E.T.P. and her group); NSF (CHE-1152755 to DLT); and NSF REU supplement (to L.S. via E.T. P.); Drexel University; and the University of Alabama for generous financial support. The X-ray diffractometer at Youngstown State University was funded by NSF Grant 0087210, Ohio Board of Regents Grant CAP-491, and by Youngstown State University. The diffractometer at Illinois State University was funded by the National Science Foundation (Grant CHE-1039689). We thank Tim Wade (Drexel University), Qiaoli Liang (the University of Alabama), and Stephen Chan (University of Delaware LIFDI facility funded by NSF MRI CHE-1229234) for MS analysis. We also thank Curt Zaleski for assistance with the X-ray diffraction data collection.

Appendix A. Supplementary data

CCDC 1048804–1048808 contain the supplementary crystallographic data for compounds LH and **1–4**. These data can be obtained free of charge from the Cambridge Crystallographic Data Centre via <https://summary.ccdc.cam.ac.uk/structure-summary?ccdc=1048804-1048808>. Supplementary data associated with this article can be found, in the online version, at <http://dx.doi.org/10.1016/j.poly.2015.10.003>.

References

- [1] I. Bertini, H.B. Gray, E.I. Stiefel, J.S. Valentine, *Biological Inorganic Chemistry*, University Science Books, Sausalito, CA, 2007.
- [2] J. Yang, A.P. Kloeck, D.E. Goldberg, F.S. Mathews, *Proc. Natl. Acad. Sci. U. S. A.* 92 (1995) 4224.
- [3] S.-I. Ozaki, M.P. Roach, T. Matsui, Y. Watanabe, *Acc. Chem. Res.* 34 (2001) 818.
- [4] A.J. Kendall, L.N. Zakharov, J.D. Gilbertson, *Inorg. Chem.* 49 (2010) 8656.
- [5] S. Sahu, L.R. Widger, M.G. Quesne, S.P. de Visser, H. Matsumura, P. Moënnelocoz, M.A. Siegler, D.P. Goldberg, *J. Am. Chem. Soc.* 135 (2013) 10590.
- [6] A. Wada, M. Harata, K. Hasegawa, K. Jitsukawa, H. Masuda, M. Mukai, T. Kitagawa, H. Einaga, *Angew. Chem., Int. Ed. Engl.* 37 (1998) 798.
- [7] A.S. Borovik, *Acc. Chem. Res.* 38 (2004) 54.
- [8] D.K. Garner, S.B. Fitch, L.H. McAlexander, L.M. Bezold, A.M. Arif, L.M. Berreau, *J. Am. Chem. Soc.* 124 (2002) 9970.
- [9] D. Natale, J.C. Mareque-Rivas, *Chem. Commun.* (2008) 425.
- [10] L. Metteau, S. Parsons, J.C. Mareque-Rivas, *Inorg. Chem.* 45 (2006) 6601.
- [11] J.C. Mareque-Rivas, S.L. Hinchley, L. Metteau, S. Parsons, *Dalton Trans.* (2006) 2316.
- [12] R.L. Lucas, M.K. Zart, J. Murkerjee, T.N. Sorrell, D.R. Powell, A.S. Borovik, *J. Am. Chem. Soc.* 128 (2006) 15476.
- [13] R.A. Allred, K. Doyle, A.M. Arif, L.M. Berreau, *Inorg. Chem.* 45 (2006) 4097.
- [14] R.A. Allred, L.H. McAlexander, A.M. Arif, L.M. Berreau, *Inorg. Chem.* 41 (2002) 6790.
- [15] E. Szajna-Fuller, B.M. Chambers, A.M. Arif, L.M. Berreau, *Inorg. Chem.* 46 (2007) 5486.
- [16] C.M. Moore, D.A. Quist, J.W. Kampf, N.K. Szymczak, *Inorg. Chem.* 53 (2014) 3278.
- [17] I. Nieto, M.S. Livings, J.B. Sacci, L.E. Reuther, M. Zeller, E.T. Papish, *Organometallics* 30 (2011) 6339.
- [18] D.L. Gerlach, S. Bhagan, A.A. Cruce, D.B. Burks, I. Nieto, H.T. Truong, S.P. Kelley, C.J. Herbst-Gervasoni, K.L. Jernigan, M.K. Bowman, S. Pan, M. Zeller, E.T. Papish, *Inorg. Chem.* (2014) 12689.
- [19] J. DePasquale, I. Nieto, L.E. Reuther, C.J. Herbst-Gervasoni, J.J. Paul, V. Mochalin, M. Zeller, C.M. Thomas, A.W. Addison, E.T. Papish, *Inorg. Chem.* 52 (2013) 9175.
- [20] K.T. Hufziger, F.S. Thowfeik, D.J. Charboneau, I. Nieto, W.G. Dougherty, W.S. Kassel, T.J. Dudley, E.J. Merino, E.T. Papish, J.J. Paul, *J. Inorg. Biochem.* 130 (2014) 103.
- [21] D.C. Marelius, S. Bhagan, D.J. Charboneau, K.M. Schroeder, J.M. Kamdar, A.R. McGettigan, B.J. Freeman, C.E. Moore, A.L. Rheingold, A.L. Cooksy, D.K. Smith, J. Paul, E.T. Papish, D.B. Grotjahn, *Eur. J. Inorg. Chem.* 2014 (2013) 676.
- [22] E.T. Papish, N.A. Dixon, M. Kumar, *Struct. Bonding* 160 (2014) 115.
- [23] N.A. Dixon, A.B. McQuarters, J.S. Kraus, J.B. Soffer, N. Lehnert, R. Schweitzer-Stenner, E.T. Papish, *Chem. Commun.* (2013) 5571.
- [24] M. Kumar, E.T. Papish, M. Zeller, A.D. Hunter, *Dalton Trans.* 40 (2011) 7517.
- [25] G. Aullón, S.M. Gorun, S. Alvarez, *Inorg. Chem.* 45 (2006) 3594.
- [26] A. Alberola, L.F. Antolin, P. Cuadrado, L.M.A. González, F.J. Pulido, *Synthesis* 3 (1988) 203.
- [27] H. Irving, R.J.P. Williams, *J. Chem. Soc. (Resumed)* (1953) 3192.
- [28] E.H. Irving, R.J.P. Williams, *Nature* 162 (1948) 746.
- [29] R.F. See, R.A. Kruse, W.M. Strub, *Inorg. Chem.* 37 (1998) 5369.
- [30] P. George, D.S. McClure, *Prog. Inorg. Chem.* 1 (1959) 418.
- [31] S.N. Oseback, S.W. Shim, M. Kumar, S.M. Greer, S.R. Gardner, K.M. Lemar, P.R. DeGregory, E.T. Papish, D.L. Tierney, M. Zeller, G.P.A. Yap, *Dalton Trans.* 41 (2012) 2774.
- [32] G.A. Jeffrey, *Crystallogr. Rev.* 9 (2003) 135.
- [33] A.D. Bond, *Chemistry - A European Journal* 10 (2004) 1885.
- [34] X. Liu, C.A. Kilner, M.A. Halcrow, *Chem. Commun.* (2002) 704.
- [35] Ž.K. Jačimović, S.B. Novaković, G.A. Bogdanović, S. Belošević, A. Jokić, V.M. Leovac, *Zeitschrift für Kristallographie - New Crystal Structures* 226 (2011) 397.
- [36] A. Hergold-Brundić, B. Kaitner, B. Kamenar, V.M. Leovac, E.Z. Ivegeš, N. Juranić, *Inorg. Chim. Acta* 188 (1991) 151.
- [37] Ž.K. Jačimović, Z.D. Tomic, G.A. Bogdanović, E.Z. Iveges, V.M. Leovac, *Acta Crystallogr. Section C* 55 (1999) 1769.
- [38] A.G. Orpen, L. Brammer, *J. Chem. Soc. Dalton Trans.* (1989) S1.
- [39] S.L. Renard, C.A. Kilner, J. Fisher, M.A. Halcrow, *Journal of the Chemical Society, Dalton Trans.* 4206 (2002).
- [40] J. Day, K.E.R. Marriott, C.A. Kilner, M.A. Halcrow, *New J. Chem.* 34 (2010) 52.
- [41] C.M. Moore, N.K. Szymczak, *Chem. Commun.* 51 (2015) 5490.
- [42] G.A. van Albada, S. Nur, M.G. van der Horst, I. Mutikainen, U. Turpeinen, J. Reedijk, *J. Mol. Struct.* 874 (2008) 41.

- [43] A.V. Khripun, N.A. Bokach, S.I. Selivanov, M. Haukka, M.D. Revenco, V.Y. Kukushkin, *Inorg. Chem. Commun.* 11 (2008) 1352.
- [44] S. Hikichi, Y. Sasakura, M. Yoshizawa, Y. Ohzu, Y. Moro-oka, M. Akita, *Bull. Chem. Soc. Jpn.* 75 (2002) 1255.
- [45] D.J. Harding, P. Harding, J. Kivnang, H. Adams, *Transition Met. Chem* 35 (2010) 521.
- [46] C.E. Housecroft, A.G. Sharpe, *Inorganic Chemistry*, Prentice Hall, UK, 2012.
- [47] C.J. Walsby, J. Telser, R.E. Rigsby, R.N. Armstrong, B.M. Hoffman, *J. Am. Chem. Soc.* 127 (2005) 8310.
- [48] C. Duboc, M.-N. Collomb, F. Neese, *Appl. Magn. Reson.* 37 (2010) 229.
- [49] B. Bennett, in: G.R. Hanson, L.J. Berliner (Eds.), "EPR of Cobalt Substituted Zinc Enzymes" in *Biological Magnetic Resonance*, vol. 29, Springer, New York, 2010, p. 345.
- [50] M. Hirai, F.P. Gabbaï, *Chemical Science* 5 (2014) 1886.
- [51] I.T. Raheem, P.S. Thiara, E.A. Peterson, E.N. Jacobsen, *J. Am. Chem. Soc.* 129 (2007) 13404.
- [52] R.R. Knowles, S. Lin, E.N. Jacobsen, *J. Am. Chem. Soc.* 132 (2010) 5030.
- [53] A. Lee, J.D. Stewart, J. Clardy, B. Ganem, *Chem. Biol.* 2 (1995) 195.